

Two-Stage Concurrent X/Ku Dual-Band GaAs MMIC Power Amplifier

Philip Zurek, Zoya Popović

Department of Electrical, Computer, and Energy Engineering
University of Colorado, Boulder, USA

philip.zurek@colorado.edu, zoya.popovic@colorado.edu

Abstract—In this work, a two-stage concurrent X/Ku dual-band MMIC power amplifier is demonstrated in a 150-nm GaAs process. A topology-specific matching technique enables high-efficiency in the two bands while also introducing intra-band and out-of-band rejection regions. The concurrent mode of operation, defined when two simultaneous input bands are amplified, is also varied over numerous input power levels to study the effect on output power, efficiency, and gain. In the CW mode of operation at 9/16.1 GHz, the power amplifier achieves a power-added efficiency of 45.5/40 % with a corresponding output power of 20.2/20.5 dBm and gain of 16.9/14.5 dB. In the concurrent CW mode at 9 and 16.1 GHz at equal output power in the two bands, the power amplifier achieves a maximum power-added efficiency of 28.4 %, with corresponding output powers of 14.3 dBm in each band and gains of 16.5 and 12.9 dB for the lower and upper bands, respectively.

Keywords—Dual band, Gallium Arsenide (GaAs), monolithic microwave integrated circuits (MMICs), power amplifiers

I. INTRODUCTION

Carrier aggregation in 5G communication standards requires simultaneous amplification of signals in multiple channels [1], [2]. For reduced circuit size compared to multiple amplifiers, and greater efficiency compared to broadband designs, multi-band power amplifiers (PAs) are an attractive option. Many dual-band hybrid amplifiers have been published at sub-6 GHz frequencies, e.g. [3]. For other applications, such as phased array radar and frequency communication bands above X-band, limited results are found in the literature. Furthermore, single-stage PAs have limited gain, but the driver stages required to achieve practical gain levels degrade efficiency and linearity. For example, the dual-band PAs in [4], [5], and [6] consist of a single-stage, while a two-stage Ka/Q dual-band PA is demonstrated in [7]. The work in [8] presents a two-stage dual-band PA covering 6–18 GHz; however, different transistors are used for different bands. Here we present a X/Ku two-stage dual-band GaAs MMIC PA, shown in Fig. 1. A comparison to current state-of-the-art designs is given in Table. 1.

Table 1. Summary of Dual-Band CW PA Performance

Ref.	Freq. (GHz)	PAE (%)	P_{out} (dBm)	Gain (dB)
[4]	7.7/14.9	24/29	34.6/34.6	11/7
[5]	6/16	55/53	26/25.5	8/7.5
[6]	5/12	58/51	28/26.7	9.5/7.7
[7]	29.5/47	38/40	22.5/22.7	17.5/15.5
[8]	5/12	58/51	28/26.7	N/A
This work	9/16.1	45.5/40	20.2/20.5	16.9/14.5

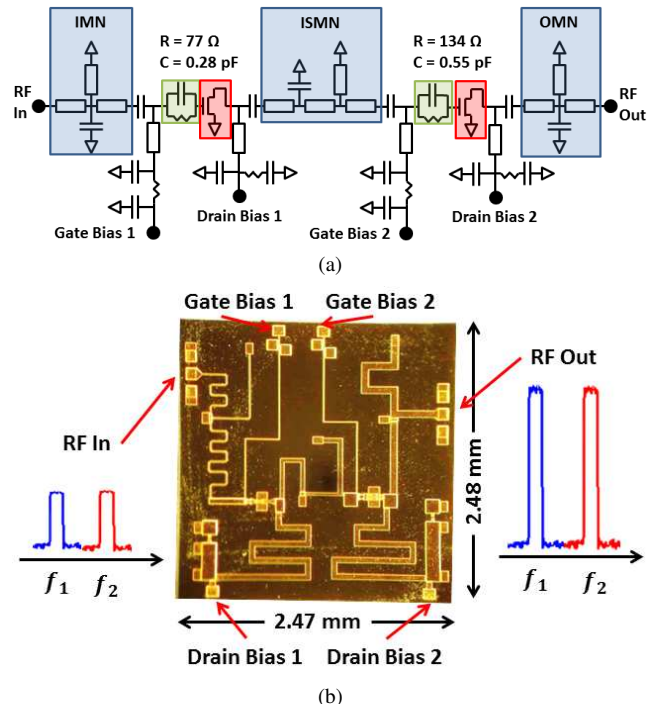


Fig. 1. Power amplifier (a) circuit diagram and (b) MMIC photograph. The same matching network and bias topology is used throughout the circuit. Concurrent signals are input at carrier frequencies $f_1 = 9$ GHz and $f_2 = 16.1$ GHz.

Design choices for this amplifier are described in Section II, followed by a comparison of simulated and measured performance in the CW and concurrent modes of operation in Sections III and IV, respectively.

II. DESIGN METHODOLOGY

The WIN Semiconductor PIH 150-nm pHEMT enhancement-mode GaAs process is chosen. In a phased array application, especially at increasingly high frequencies, the efficiency of each element is important because the number of elements per unit area increases. Therefore, at the targeted X and Ku-bands of operation, heat dissipation is an important factor to consider, and hence, efficiency is optimized during the design procedure. The second stage is sized such that it can deliver at least $P_{out} = 20$ dBm ($4 \times 100 \mu\text{m}$), with the first stage sized for a 1:4 staging ratio ($2 \times 50 \mu\text{m}$).

A deep Class-AB mode of operation (10% of I_{max}) is chosen as a trade-off between efficiency and P_{out} . In order to achieve a high-efficiency when either one or both signals

are present, the input, interstage, and output matching networks have to provide an appropriate match with low loss. Broadband and low-loss gate and drain bias tees are included in the load and source pull simulations. Fig. 2 shows the load-pull contours of the output stage at the two frequencies. The output matching network impedance is shown in red, demonstrating a poor match in the intra-band region.

Note the spacing of the power and efficiency contours and the corresponding dip in the intra-band region, as discussed in detail in the remainder of the paper. An analogous procedure is used for determining required impedances at the input, and between stages. The matching networks are designed using linear simulations with a topology consisting of three sections of transmission line, with a capacitive shunt element and inductive shunt element, as depicted in Fig. 1. Finally, full-wave electromagnetic and harmonic-balance simulations are performed to give final circuit performance.

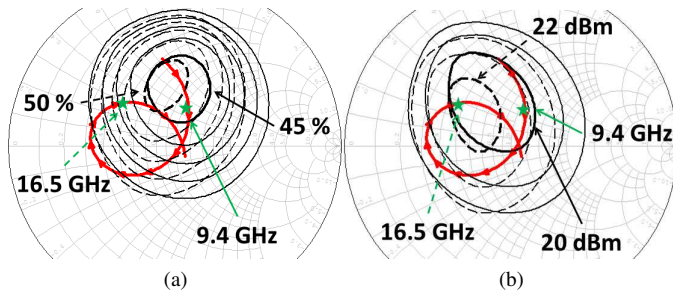


Fig. 2. Simulated (a) PAE and (b) P_{out} load-pull contours for the output matching network, at the reference plane after the biasing network. Solid black circles are for 9.4 GHz and dashed for 16.5 GHz. Step size for PAE is 5% and 1 dB for P_{out} . The red curve shows simulated impedances from 8 to 18 GHz presented by the output matching network, with 9.4 GHz ($\Gamma = 0.08 + j0.20$) and 16.5 GHz ($\Gamma = -0.35 + j0.25$) marked.

Stability for this PA with two widely spaced frequency bands is confirmed in multiple ways. From DC through the third harmonic, it is ensured that $K > 1$. The NI-AWR linear Nyquist stability criterion is also used. For both of these tests, the input and output terminations of the power amplifier are swept, while the bias source termination is also varied over reasonable values to account for a real supply. Next, using the foundry's nonlinear model at the chosen bias level of $V_d = 4V$ and $V_g = 0.45V$ for both stages, corresponding to a drain current of 5.54 and 21.7 mA for the first and second stage respectively, for both devices, a linear model of the transistor is extracted. With this model, g_m and C_{gd} are increased by 30% while C_{gs} is decreased by 30% to model a worst-case stability condition from a process variation point of view [9]. Finally, the linear model is used to perform a loop-gain analysis as a final check of design stability over port terminations and bias impedances. The final stability networks are indicated in Fig. 1.

III. CW MEASUREMENTS

An on-chip TRL kit is used with an Agilent E8364C PNA for calibration. The MMIC is mounted onto a CuMo carrier using conductive silver epoxy, with four 1 nF capacitors, and probed. Small-signal measurements are recorded and shown

in Fig. 3. This figure also shows simulated small-signal measurements for comparison, demonstrating good agreement and a slight downward frequency shift of 400 MHz for both bands (about 4.3/2.4%), likely due to matching elements, such as capacitors, being sensitive to process variations. Small-signal measurements are confirmed with a scalar setup for power measurements, by backing off the power. The large-signal measurement frequency sweep is shown in Fig. 4. This shows the maximum saturated power-added efficiency (PAE) at each frequency, alongside the corresponding P_{out} and gain. A power sweep is performed comparing the two frequencies with highest efficiency in both the simulated and measured cases in Fig. 5.

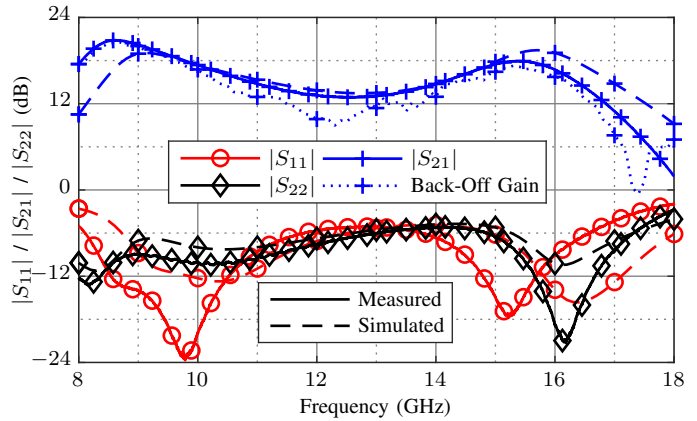


Fig. 3. Small-signal simulated and measured S -parameters over frequency. Measurements are done with a PNA, and also with a scalar power measurement setup ("Back-Off Gain"), confirming agreement.

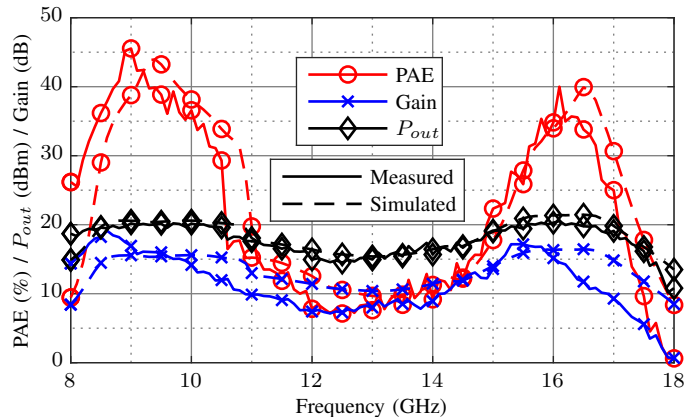


Fig. 4. Simulated and measured CW performance of the PA over frequency. Peak simulated/measured PAE values are observed at 9.4/9.0 and 16.5/16.1 GHz.

IV. CONCURRENT CW MEASUREMENTS

To measure true PA performance in the concurrent mode, the power in the two bands needs to be measured with separate power meters. A scalar test bench that accomplishes this task using power splitters and bandpass filters, is shown in the block diagram in Fig. 6.

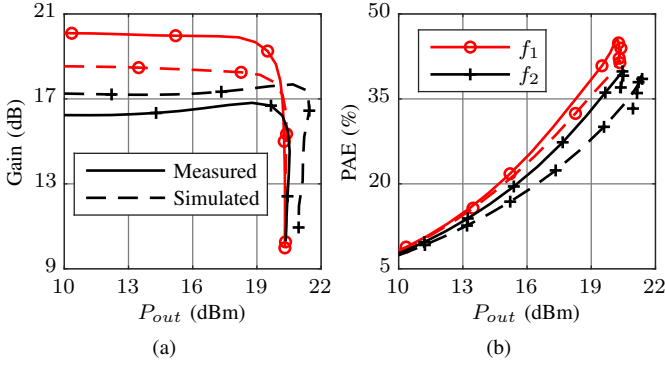


Fig. 5. Simulated ($f_1=9.4$ GHz and $f_2=16.5$ GHz) and measured ($f_1=9.0$ GHz and $f_2=16.1$ GHz) CW (a) gain and (b) PAE of the PA over P_{in} for both f_1 and f_2 .

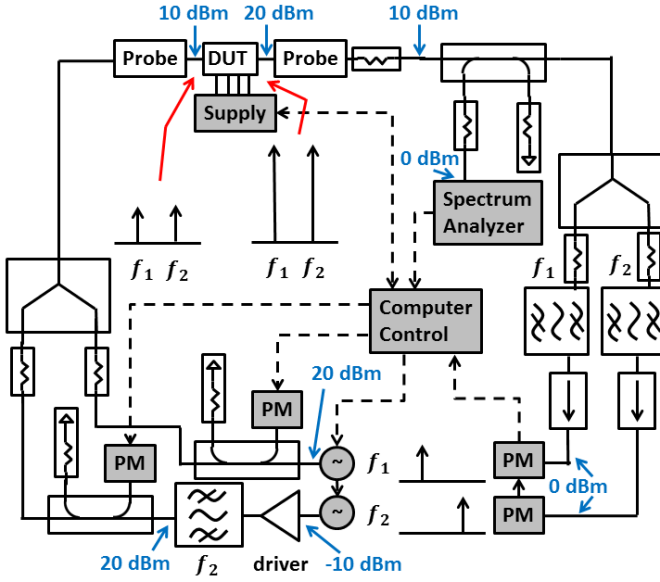


Fig. 6. Setup block-diagram used to make concurrent CW measurements. Two sources provide tones which are each measured through a coupler. These are combined and input to the PA. The signal is then split and the two tones isolated before being measured with a power meter.

Because 9 and 16.1 GHz are 7.1 GHz apart, two sources must be used to generate the concurrent signal. A driver is cascaded with one source to generate enough power, while harmonics are eliminated with a bandpass filter. A calibration is performed from the probe input and the coupler output along these two paths to measure P_{in} . These CW signals are combined with a resistive power combiner and additional attenuators for matching, measured to be -15 dB or better at the input. Immediately at the output an attenuator is present to present a measured output match of -15 dB or better. The output signal is coupled to a spectrum analyzer while the thru signal is split. The split signal travels through a bandpass filter, which has an attenuator and isolator at either end to ensure a good match, before being measured by a power meter. Because one filter operates from 8 - 13.9 GHz, and the other from 14.8 - 18.5 GHz, this setup ensures that only in-band power is measured.

The concurrent mode of operation is analyzed and results

summarized in Fig. 7. Relative input power levels are defined from the CW $P_{in}(f)$ value corresponding to the maximum PAE(f). At f_1/f_2 this is measured as approximately 3/6 dBm. In the legend of Fig. 7, A and B correspond to a 6 dB back-off value while C and D correspond to the nominal $P_{in}(f)$ (0 dB back-off). When two CW tones are present, four power measurements can be made: $P_{in}(f_1)$, $P_{in}(f_2)$, $P_{out}(f_1)$, and $P_{out}(f_2)$. Therefore, a self (f_n/f_n) and cross (f_n/f_m) measurement can be defined for gain (B and D) and P_{out} (A and C) over P_{in} .

The results of Fig. 7 show that as cross- P_{in} increases, self-gain, self- P_{out} , and cross-gain decrease while cross- P_{out} increases. As this happens, neither signal is able to dominate in the amplification, and because the amplifier is limited in the total P_{out} it can produce, concurrent-mode gain and P_{out} must reduce accordingly. The authors note that some discrepancies between measurements and simulations may be due to the nonlinear model not correctly predicting concurrent operation.

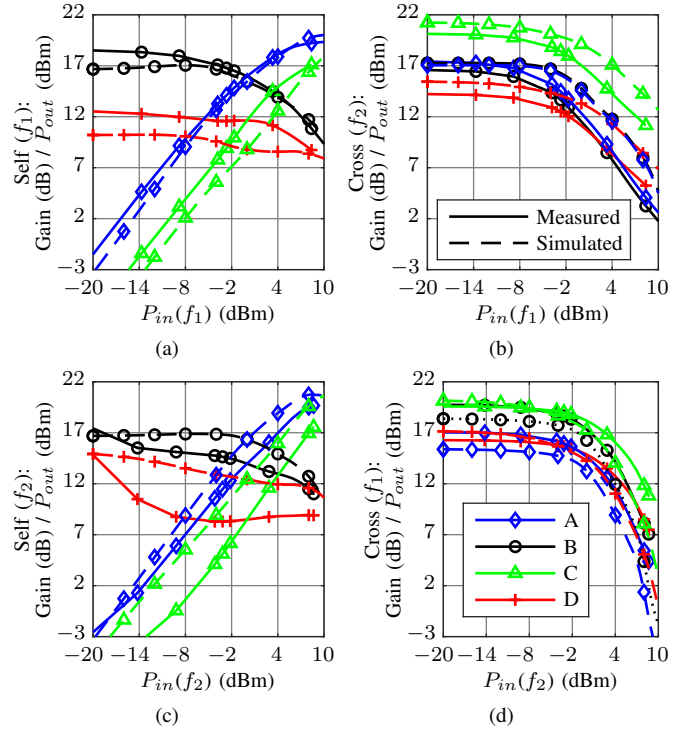


Fig. 7. Simulated ($f_1=9.4$ GHz and $f_2=16.5$ GHz) and measured ($f_1=9.0$ GHz and $f_2=16.1$ GHz) concurrent mode self and cross-gain and P_{out} of the PA over several P_{in} . The legend in (d) corresponds to: A - P_{out} , 6 dB backoff; B - gain, 6 dB backoff; C - P_{out} , 0 dB backoff; and D - gain, 0 dB backoff. The top row (a) and (b) shows self results over $P_{in}(f_1)$ for a constant $P_{in}(f_2)$. Similarly, the bottom row (c) and (d) shows cross results over $P_{in}(f_2)$.

Because one cannot isolate the PAE of just one band or the other during concurrent operation, a three-dimensional figure could be used to illustrate the simultaneous effect of both bands on PAE. A similar analysis can be performed for P_{out} . Measured data is summarized as a heat map in Fig. 8, where PAE is defined as:

$$PAE = \frac{P_{out,1} + P_{out,2} - P_{in,1} - P_{in,2}}{P_{DC}} \quad (1)$$

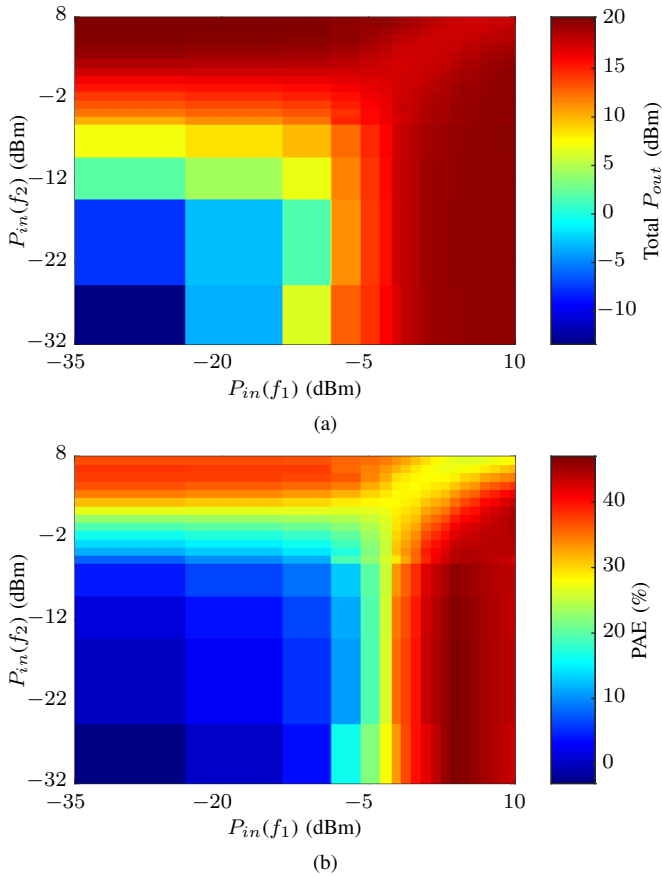


Fig. 8. Heat map illustrating the measured $f_1=9.0$ GHz and $f_2=16.1$ GHz concurrent mode of operation of (a) Total P_{out} and (b) PAE over P_{in} .

The heat map degenerates to the CW case at the two axes where the other band is turned off. There exists a saddle point in the PAE in a region where P_{out} in both bands is about equal. The corresponding saddle point in the P_{out} plot shows a slightly lower value than the CW case.

For the same P_{out} in each band, the amplifier simulated and measured performance is shown in Fig. 9. These curves follow the ones for the CW case. As compared to simulation, it is noted that the gain of the lower band is higher and the upper band lower, possibly due to either process variations (because the upper band sees decreased performance due to slight matching issues) or the nonlinear model not correctly predicting concurrent operation (because of the results of Fig. 7). In this figure at the maximum PAE point, $P_{in}(f_1)$ and $P_{in}(f_2)$ are about 5 dB lower than their respective CW values.

V. CONCLUSION

This work presents the results of a two-stage X/Ku-band GaAs MMIC power amplifier operating in CW and concurrent-CW modes of operation. Measured PAE is reported as 45.4/40%, with a corresponding $P_{out} = 20.2/20.7$ dBm and a gain of 16.9/14.5 dB at 9/16.1 GHz. This amplifier compares well to state-of-the-art designs reported in the literature, while also providing an analysis of the concurrent mode of operation at these frequencies with a multi-stage design for the first time. It is concluded that nonlinear models could be improved to better capture concurrent modes of operation.

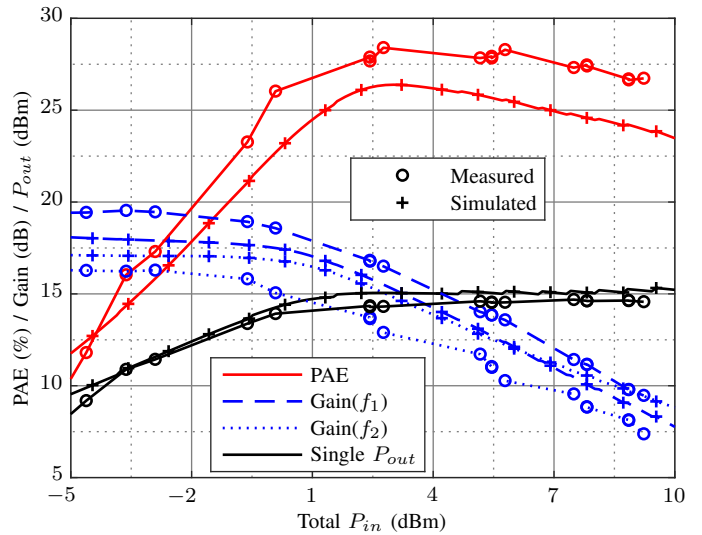


Fig. 9. Simulated ($f_1=9.4$ GHz and $f_2=16.5$ GHz) and measured ($f_1=9.0$ GHz and $f_2=16.1$ GHz) amplifier performance when both bands output equal power.

ACKNOWLEDGMENTS

The authors would like to thank Christopher Galbraith at the MIT Lincoln Laboratory for his helpful discussions and collaborations in this work.

REFERENCES

- [1] Z. Shen, A. Pappasakellariou, J. Montojo, D. Gerstenberger, and F. Xu, "Overview of 3GPP LTE-advanced carrier aggregation for 4G wireless communications," *IEEE Communications Magazine*, vol. 50, no. 2, pp. 122–130, February 2012.
- [2] S. A. Bassam, W. Chen, M. Helaoui, and F. M. Ghannouchi, "Transmitter architecture for CA: carrier aggregation in LTE-advanced systems," *IEEE Microwave Magazine*, vol. 14, no. 5, pp. 78–86, July 2013.
- [3] G. Nikandish, E. Babakrpur, and A. Medi, "A harmonic termination technique for single- and multi-band high-efficiency class-F MMIC power amplifiers," *IEEE Trans. Microw. Theory Techn.*, vol. 62, no. 5, pp. 1212–1220, May 2014.
- [4] R. Quaglia, V. Camarchia, and M. Pirola, "Dual-band GaN MMIC power amplifier for microwave backhaul applications," *IEEE Microwave and Wireless Components Letters*, vol. 24, no. 6, pp. 409–411, June 2014.
- [5] A. Alizadeh, M. Frounchi, and A. Medi, "Dual-band design of integrated class-J power amplifiers in GaAs pHEMT technology," *IEEE Transactions on Microwave Theory and Techniques*, vol. 65, no. 8, pp. 3034–3045, Aug 2017.
- [6] G. Nikandish, E. Babakrpur, and A. Medi, "A harmonic termination technique for single- and multi-band high-efficiency class-F MMIC power amplifiers," *IEEE Transactions on Microwave Theory and Techniques*, vol. 62, no. 5, pp. 1212–1220, May 2014.
- [7] G. Lv, W. Chen, X. Chen, and Z. Feng, "An energy-efficient Ka/Q dual-band power amplifier MMIC in 0.1- μ m GaAs process," *IEEE Microwave and Wireless Components Letters*, vol. 28, no. 6, pp. 530–532, June 2018.
- [8] K. Choi, H. Park, M. Kim, J. Kim, and Y. Kwon, "A 6–18-GHz switchless reconfigurable dual-band dual-mode PA MMIC using coupled-line-based diplexer," *IEEE Transactions on Microwave Theory and Techniques*, vol. 66, no. 12, pp. 5685–5695, Dec 2018.
- [9] C. Campbell, *Microwave Monolithic Power Amplifier Design*. John Wiley & Sons, Inc., 2013. [Online]. Available: <https://onlinelibrary.wiley.com/doi/abs/10.1002/047134608X.W8180>